Journal Pre-proof

Numerical simulations of derived URM-RC buildings: assessment of strengthening interventions with RC

Gonçalo Correia Lopes, Nuno Mendes, Romeu Vicente, Tiago Miguel Ferreira, Miguel Azenha

Please cite this article as: G.C. Lopes, N. Mendes, R. Vicente, T.M. Ferreira, M. Azenha, Numerical simulations of derived URM-RC buildings: assessment of strengthening interventions with RC, *Journal of Building Engineering*, https://doi.org/10.1016/j.jobe.2021.102304.

This is a PDF file of an article that has undergone enhancements after acceptance, such as the addition of a cover page and metadata, and formatting for readability, but it is not yet the definitive version of record. This version will undergo additional copyediting, typesetting and review before it is published in its final form, but we are providing this version to give early visibility of the article. Please note that, during the production process, errors may be discovered which could affect the content, and all legal disclaimers that apply to the journal pertain.

CRediT author statement

Gonçalo Correia Lopes: Conceptualization; Methodology; Investigation; Software; Writing - Original Draft; Visualization. **Nuno Mendes:** Conceptualization; Resources; Software; Investigation; Validation. **Romeu Vicente:** Conceptualization; Resources; Writing - Review & Editing. **Tiago Miguel Ferreira:** Conceptualization; Writing - Review & Editing. **Miguel Azenha:** Conceptualization; Resources; Writing - Review & Editing.

Numerical simulations of derived URM-RC buildings: assessment of strengthening interventions with RC

Gonçalo Correia Lopes[1], Nuno Mendes[2], Romeu Vicente[1], Tiago Miguel Ferreira[2], Miguel Azenha[2]

[1]RISCO – Aveiro research centre for RIsks and Sustainability in COnstruction, University of Aveiro, Civil Engineering Department, Campus Universitário de Santiago, 3810-193 Aveiro, Portugal.

[2]ISISE, Institute of Science and Innovation for Bio-Sustainability (IB-S), University of Minho, School of Engineering, Civil Engineering Department, Azurém Campus, 4800-058 Guimarães, Portugal.

e-mails: gclopes@ua.pt, nunomendes@civil.uminho.pt, romvic@ua.pt, tmferreira@civil.uminho.pt, miguel.azenha@civil.uminho.pt

Corresponding author: Gonçalo Correia Lopes, e-mail: gclopes@ua.pt, telephone number: +351 914729528

Abstract

The use of reinforced concrete (RC) in retrofitting interventions on existing unreinforced masonry (URM) buildings has been spreading all over the world since the beginning of the twentieth century. However, many of these mixed URM–RC buildings have revealed to be particularly vulnerable to seismic action, and their inherent complex structural behaviour is still understudied. In fact, the interaction effects from coupling RC structural elements to URM loadbearing walls is still a contentious issue for most of the research community.

In this context, the present paper represents a steppingstone for the thorough understanding of the influence of strengthening interventions with RC in existing URM buildings, namely, regarding the addition of reinforcement layers on the horizontal diaphragms, and the insertion of ring beams at the roof level.

This article describes a finite element nonlinear static analysis of a representative URM-RC building, before and after the introduction of the RC strengthening elements. The models used in these finite element-based analyses have been automatically created from BIM models correspondent to two full-scale prototype buildings (unstrengthened and strengthened configurations), analysed experimentally in a shaking table test campaign performed at the European Centre for Training and Research in Earthquake Engineering (EUCENTRE).

The obtained results have been calibrated based on experimental results and compared with other numerical results obtained resorting to a macroelement-based model, found in the literature. As presented and discussed in this article, the refined finite element models have provided a better approximation of the experimental seismic behaviour of the building than the macroelement models. Plus, the refined finite element models have allowed to assess the influence of each strengthening element when applied separately.

Keywords: mixed URM–RC buildings; RC strengthening actions; seismic retrofit; pushover analysis; BIM

1. Introduction

The present article falls within the scope of research work on the evaluation and reduction of the seismic vulnerability of existing unreinforced masonry (URM) structures to which new reinforced concrete (RC) structural elements have been added.

This mixed construction typology – designated as "derived mixed URM–RC buildings" [1] – arose at the beginning of the twentieth century, driven by the development and progressive use of RC. The implementation of such practices, mainly in strengthening/retrofitting interventions of existing URM buildings, has been spread all over the world, particularly during past reconstruction processes that took place after significant earthquakes, and due to numerous recommendations given in certain building codes. However, some of these derived mixed URM–RC buildings revealed to be particularly vulnerable to seismic loads, and only in recent years researchers have started to turn their attention to the seismic vulnerability of mixed URM–RC structures, by studying and observing their particular damage patterns, mechanisms, and interaction effects from coupling RC structural elements to URM loadbearing walls. As summarised by Correia Lopes et al. [1], among the reasons of the eventual inadequacies associated with the considered techniques are the connections' effectiveness, the discrepancy between the stiffness and weight of RC and masonry, any unfavourable redistribution of stresses and/or the eccentricity of the loads during seismic actions.

Moreover, the existing research involving the thorough simulation of shaking table tests on full-scale derived URM-RC building typologies is still very limited, particularly regarding the investigation of the variation of the seismic response depending on different strengthening interventions using RC.

In this topic, Tomaževič et al. [2] carried out a shaking table test campaign on four 1/5 scaled three-storey models, with different internal structure. Two of the four models had an inner RC column and two RC beams, while in the other two models the internal column has been replaced by two perpendicular masonry walls. Jurukovsky et al. [3] conducted shaking table tests on 1/3 scaled four-storey models to investigate the seismic behaviour of a masonry structure with one RC frame at the ground floor, and to examine the effect of two strengthening solutions – the addition of external RC walls and the insertion of a central RC core. More recently, Mazzon et al. [5] carried out shaking table tests on two 2/3 scaled two-storey models: the first was tested in unreinforced conditions, while the second was strengthened using grout injections. Vintzileou et al. [7] performed biaxial shaking table tests on a 1/2 scaled two-storey model before and after interventions, consisting in grouting injections, addition of a second pavement on top of the existing timber diaphragm and improved connections of the floors to the walls.

As pointed out by Senaldi et al. [8], "the lack of comprehensive testing campaigns on full-scale specimens is evident". In this context, the most significant and extensive testing campaign on full-scale mixed URM-RC buildings has been performed at the European Centre for Training and Research in Earthquake Engineering (EUCENTRE), which has provided particularly relevant experimental information applicable for validating modelling approaches for these type of structures [8–12].

The EUCENTRE experimental campaign included preliminary characterization of masonry wallettes to obtain masonry properties, a set of in-plane cyclic tests on large masonry piers and spandrels, and shaking table testing on three full-scale buildings, with identical geometry and materials, designed to be representative of different strengthening interventions on the same building geometry.

The first prototype building tested (designated as Building 1) was representative of existing unstrengthened stone masonry structures with flexible timber diaphragms, without any specific anti-seismic design nor structural detailing, thus serving as the reference unstrengthened configuration. In the second and third buildings (designated as Building 2 and Building 3), strengthening interventions were simulated on structures theoretically identical to the first one, improving the wall-to-floor and wall-to-roof connections and increasing diaphragm stiffness. In Building 2, a steel ring beam at the floor level and a reinforced masonry ring beam at the roof level were used to improve the connections between diaphragms and walls [13]. In the Building 3, an RC ring beam was used to

improve the diaphragm connection to the walls at roof level, and an RC collaborating slab and multi-layer plywood panels were used to stiffen the floor and roof diaphragms, respectively [8].

In addition to the shaking table tests, nonlinear static (pushover) analyses and nonlinear dynamic (time history) analyses of equivalent frame models (EFM) with macroelements were performed (using the Tremuri software) to simulate the seismic response of the strengthened prototypes [11,14]. In comparison with the original non-strengthened configuration, Building 3 was able to withstand a much stronger shaking action, exploiting the in-plane capacity of the walls. The addition of the ring beam has also significantly improved the coupling effect of masonry spandrels, enhancing the in-plane shear capacity of the walls, and increasing lateral strength and stiffness [8].

Given the relevance of the EUCENTRE campaign in the scope of the present investigation – derived mixed URM–RC buildings –, the same prototype buildings will serve as the basis for the case study buildings analysed in the next sections. The focus will be placed on the comparison of the seismic performance of the Building 1 (an "original" URM building) and Building 3 (a "derived" mixed URM-RC building), both described in Section 2. The non-consideration of Building 2 in the present article is due to the fact that its strengthening did not involve RC elements, hence rendering out of the scope of the present research goals. Section 3 will be devoted to the replication of the numerical analysis performed using equivalent frame macroelement models, this time using nonlinear finite element models (FEM) in order to attain a better approximation of the seismic behaviour observed during the experiment shaking table tests. For that purpose, modal analyses and pushover analyses will be performed using the DIANA software, and calibrated based on the experimental results. Furthermore, once the numerical models of Buildings 1 and 3 are calibrated, four additional building models will be considered in Section 4 to compare the influence of each strengthening intervention separately.

2. Case study buildings – real scale experimental tests

The two URM prototypes share the same global geometry, which corresponds to that of a single-room two-storey building with a simply supported timber floor and a pitched roof (see Fig. 1). The direction of the shaking table motion is parallel to the longitudinal walls (E and W façades), coinciding with the Y-axis (oriented $\overrightarrow{SN}$).
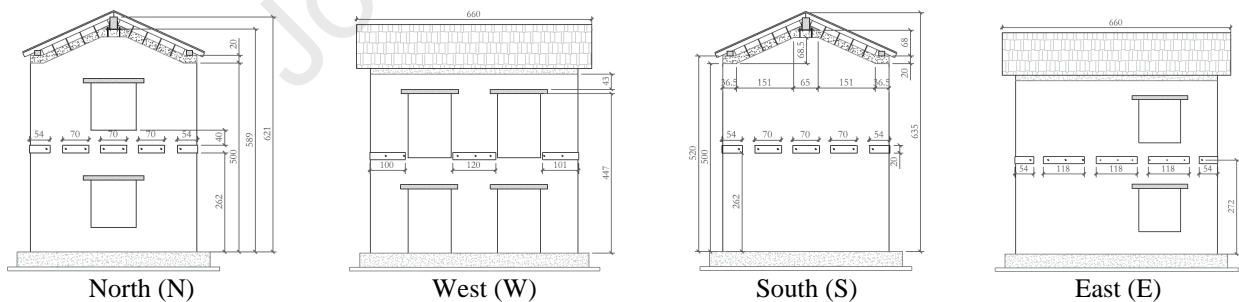

Fig. 1. Elevation views of the walls of the Building 3 specimen (dimensions in centimetres) [8]

The structural walls consisted of double-leaf stone masonry, with a nominal thickness of 32 cm, in which the two leaves of undressed stones were simply built close to each other and the remaining irregular gaps between filled with small stones and mortar. Through stones were present only at the corner angles and in the vicinity of wall openings [10]. Timber lintels with 32 cm wide and 12 cm high were present on all openings.

The floor and roof structures were designed to be representative of real buildings with typical construction details (see Fig. 2). The floor structure was made of 12 cm × 16 cm high pinewood joists placed every 50 cm with 3 cm thick planks simply nailed to the joists. Additional masses were laid on the floor after the building was fixed to the table in order to simulate a regularly distributed load equal to 31.38 kN (3.2 tons) [9].

The roof structure included one 20 cm × 32 cm ridge beam and 8 cm × 12 cm rafters every 50 cm, forming the two pitches with 3 cm thick planks. Building 1 also had two-segmented 32 cm × 12 cm spreader beams on the top of the longitudinal walls (which has not been included in the Building 3). The roof was then covered with clay tiles, each of those nailed to the timber structure to prevent possible fall-off during the tests, totalling a weight of 12.32 kN [9,13].
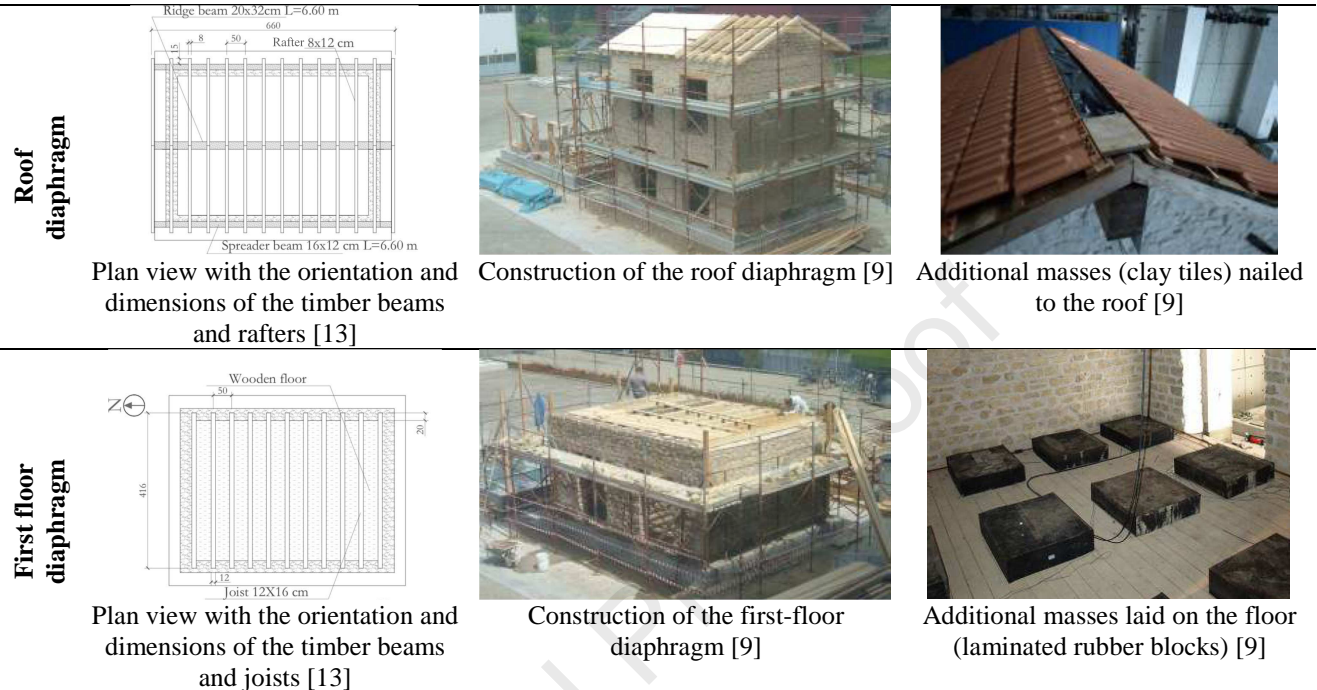
Roof diaphragm		
Plan view with the orientation and dimensions of the timber beams and rafters [13]	Construction of the roof diaphragm [9]	Additional masses (clay tiles) nailed to the roof [9]
First floor diaphragm		
Plan view with the orientation and dimensions of the timber beams and joists [13]	Construction of the first-floor diaphragm [9]	Additional masses laid on the floor (laminated rubber blocks) [9]

Fig. 2. Construction details of the first floor and roof levels of Building 1

Furthermore, the fundamental difference between the building prototypes 1 and 3 lies in the inclusion of strengthening elements in Building 3, see Fig. 3. The original flexible floor structure has been strengthened with a 7 cm thick RC collaborating slab, thus creating a mixed RC–timber structure connected to the walls by external anchoring steel plates and through bars anchored in the RC slab. The roof pitches were stiffened by the application of 3 layers of spruce plywood panels, each 2.1 cm thick, and by the insertion of a 32 cm × 20 cm RC ring beam, cast at the top of the external loadbearing walls (see reference [8] for further details).
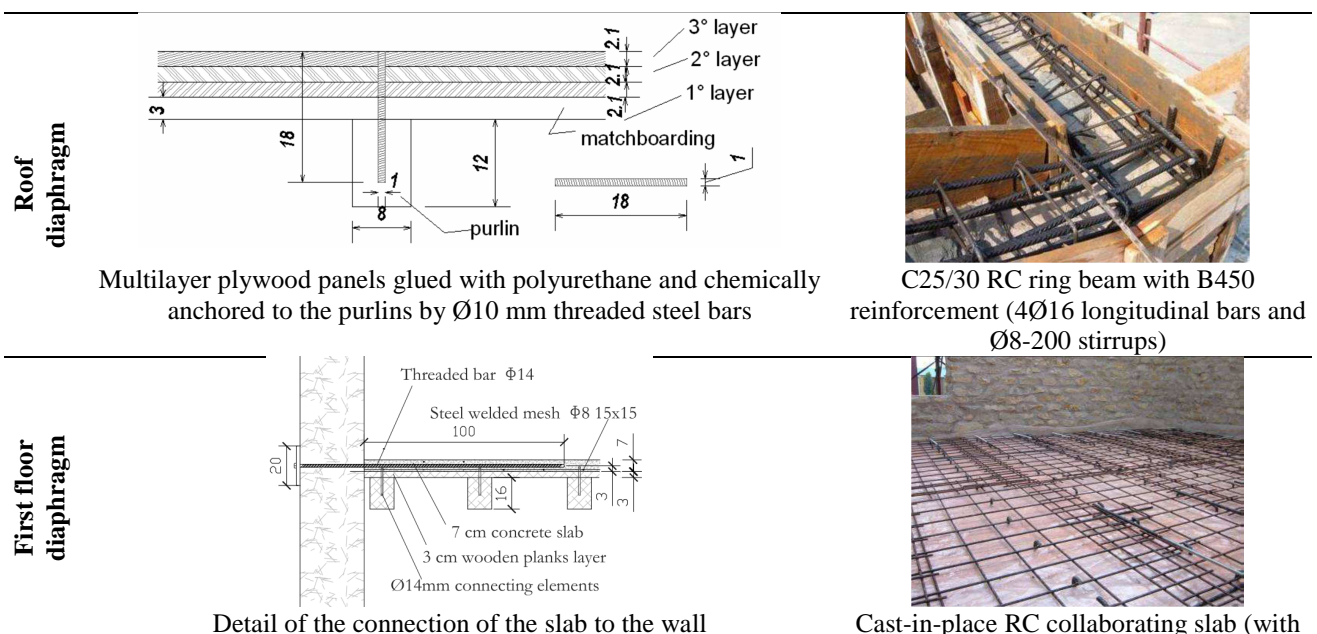
Roof diaphragm		
Multilayer plywood panels glued with polyurethane and chemically anchored to the purlins by Ø10 mm threaded steel bars		C25/30 RC ring beam with B450 reinforcement (4Ø16 longitudinal bars and Ø8-200 stirrups)
First floor diaphragm		
Detail of the connection of the slab to the wall		Cast-in-place RC collaborating slab (with

steel welded mesh Ø8-150)

Fig. 3. Scheme of the strengthening intervention applied to Building 3 (adapted from [8])

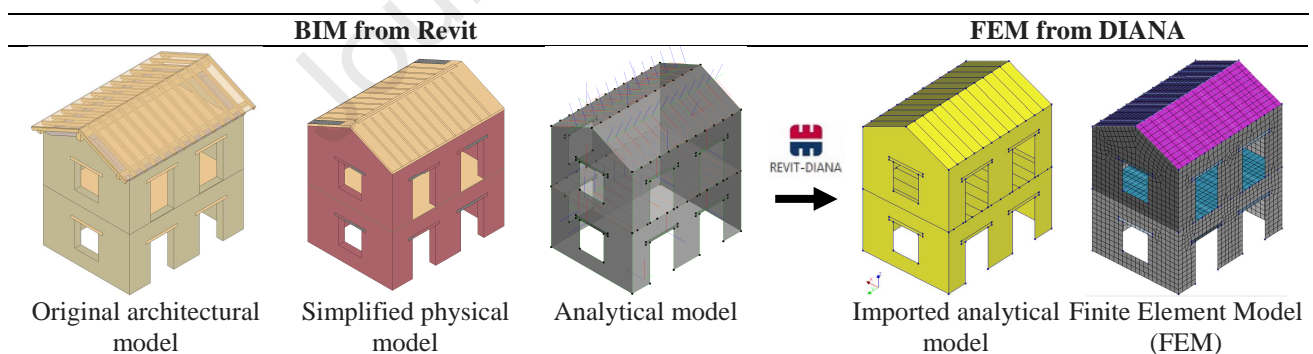# 3. Finite element modelling approach

3.1. Modelling considerations

In the present work, a BIM environment has been employed in order to streamline the modelling process of the buildings, taking advantage of the interoperability between the BIM modelling software and the numerical analysis software.

The BIM architectural models of the prototype buildings were developed using the software Revit [15] based on the 2D drawings from the previous section. Naturally, these models can store valuable information about each modelled object (e.g., materials' physical properties, dimensions, nomenclature, etc.).

Then, the original architectural models were simplified to allow the automatic generation of adequate analytical models, minimizing the need of further manual adjustments: (i) the central axes of the floor joists and roof rafters were placed coplanar with the respective diaphragm; (ii) the walls were vertically extended to intersect the roof pitches; (iii) the overhang portions of the roof were trimmed to the planes of the walls; (iv) the location of the ring beam was slightly adjusted to coincide to the perimetral edges of the roof.

The Revit analytical models are composed of analytical planes and lines representing planar elements (walls, diaphragms, etc.) and linear elements (beams, columns, etc.), respectively. Finally, the analytical models from Autodesk Revit have been exported to the structural analysis software DIANA v10.3 [16] via the Revit-DIANA plugin v17.0 [17]. The output of the Revit plugin is a python file (script) that can be read by DIANA, thus avoiding the need to recreate the structural models manually. The floor and roof diaphragms (as well as the lintels embedded in the walls) in Revit were converted into DIANA "Sheets", and the beam elements (RC ring beam and timber beams/joists/rafters) were converted into DIANA "Wires", maintaining the original dimensions (thicknesses and cross-sections). These models are illustrated in Fig. 4.

BIM from Revit				**FEM from DIANA**
Original architectural model	Simplified physical model	Analytical model	Imported analytical model	Finite Element Model (FEM)

Fig. 4. Scheme of the models from BIM to FEM

Then, additional vertical loads were applied on the diaphragms to match the ones from the experimental tests. The boundary conditions, namely the three translation and three rotation components between the foundation and the soil, were defined as fixed.

In addition, in order to accurately replicate the geometry of the real prototype buildings, slight adjustments have been introduced in the BIM analytical models of Buildings 1 and 3, by selecting the Edge Horizontal Alignment option in Revit to 'Auto-Detect' or to 'Projection', respectively (see Fig. 5).

In the modelling of Building 1 (the reference unstrengthened configuration), the floor and roof diaphragms are disconnected from the four walls and from the two gable walls, respectively. That is, the first-floor diaphragm is supported by the timber joists (which are fixed to the walls at their ends), and the roof diaphragm is supported by the roof rafters, ridge beam and longitudinal walls (see left

part of Fig. 5). Although the timber joists are usually simply supported by the masonry walls, in the adopted macro-modelling approach, aiming at evaluating the global behaviour of the structure, all the connections between adjoining elements (timber joists/rafters, roof/floor diaphragms and walls) were considered perfect (the sliding at the connections is not considered). This assumption was adopted for both buildings, since no relative displacements at the connections nor local collapses, due to the lack of connection between roof/floor and walls, were observed in the shake tables tests (visual inspection). Moreover, it should be noticed that the test setups do not include monitoring devices in between the roof/floor and walls connections to estimate the parameters involved in the behaviour of this type of complex connections (for example, the non-linear stiffness in compression and tension, and the parameters of a failure based on the and Mohr-Coulomb's friction law). Despite this aspect, the flexibility of the timber floor, which also plays an important role in the seismic behaviour of existing masonry buildings, was considered.

In the modelling of Building 3 (the strengthened configuration), a perfect connection between the RC ring beam, floor/roof diaphragms, and masonry walls was assumed in order to simulate the action of the RC collaborating slab and the steel connectors at the floor level, as well as the RC ring beam and roof strengthening layer at the roof level (right part of Fig. 5). Accordingly, the steel connectors of Building 3 were not explicitly modelled since no experimental data on the linear and non-linear behaviour of the connections are available, for example, to simulate the sliding at the threaded bar/concrete interface. Moreover, Building 3 did not reveal any signs of damage on the RC elements during the experimental tests. Thus, to simulate the RC elements (collaborating slab and ring beam), in a simplified manner, it was only considered an elastic linear behaviour and without the steel reinforcement since no damage is expected in these elements. According to the experimental results, the damage has occurred only on the URM walls, whereby it was opted to simulate the nonlinear behaviour only on the masonry elements.
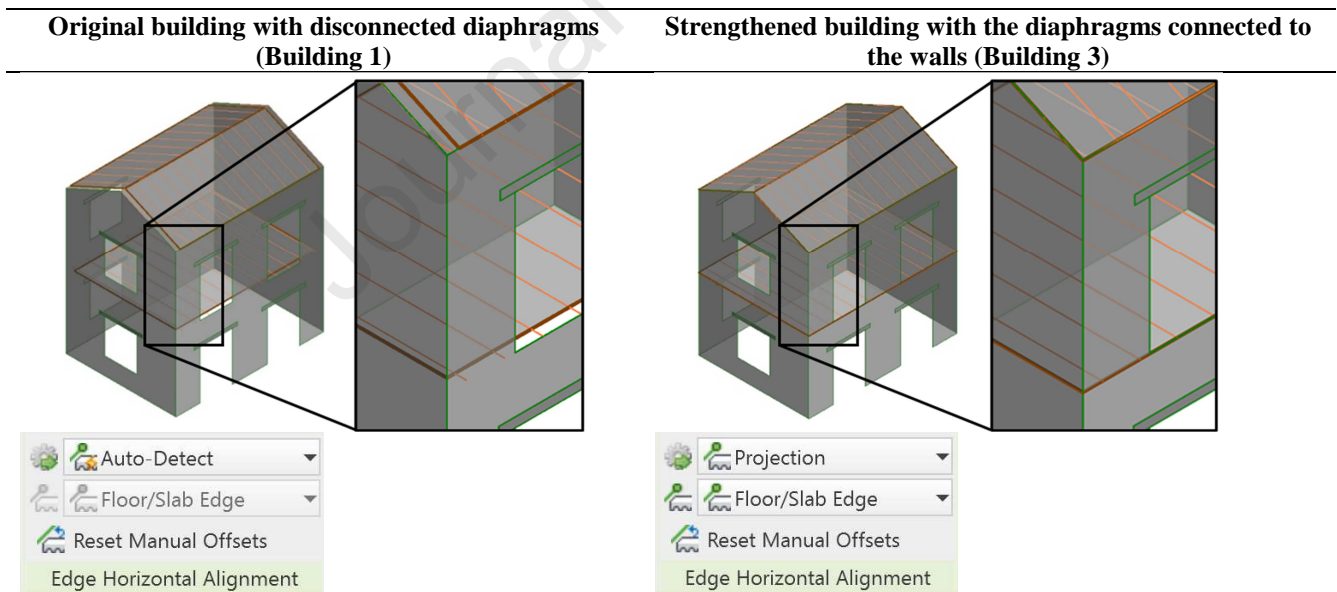
Original building with disconnected diaphragms (Building 1)	Strengthened building with the diaphragms connected to the walls (Building 3)

Fig. 5. Analytical model adjustments considered in Revit for the connections of the diaphragms to the walls

3.2. Finite element models

As stated previously, the chosen structural analysis software was the DIANA v10.3 [16]. The software DIANA (Displacement method ANAlyser) is an extensive multi-purpose finite element program with different possibilities for the constitutive models of masonry materials.

Once imported the analytical model from Revit, the structural walls and diaphragms were discretised using dominantly linear quadrilateral curved shell elements, with edge sizes limited to 0.2 m.

Based on the adopted numerical modelling approach (macro-modelling), curved shell elements have been selected to simulate the masonry walls. Although the walls are double-leaf stone masonry walls, no disintegration of the masonry was observed in the shake table tests.

Regarding the discretization of the element order, the default element order generated by the mesher was set to "linear". According to Lourenço & Pereira [18], "linear elements are more constrained and are less prone to spurious movements than quadratic elements, in the presence of very low stiffness due to extensive inelastic behaviour".

The basic variables in the nodes of the shell elements correspond to their five degrees of freedom: three translations (u_x, u_y, u_z) and two in-plane rotation degrees (ϕ_x, ϕ_y). The derived variables are the strains, the Cauchy stresses and the generalized moments and forces [19].

Different finite element classes have been used for the different structural elements [19]:

- the masonry walls were modelled with four-node quadrilateral isoparametric curved shell elements (Q20SH) with a 2×2 integration scheme over the element area and 5-points through the thickness (useful for the nonlinear analysis);
- the original timber diaphragms and the timber lintels were also modelled with regular curved shell elements (Q20SH) but with the default 3-point integration through the thickness;
- the timber diaphragms with a composite arrangement (timber + RC or timber + plywood) were modelled with eight-node quadrilateral isoparametric curved layered shell elements (CQ40L) with a 2×2 integration scheme over the surface and 3-points through the thickness. The number of layers used was 2, one for each material, with its own material properties and with separated numerical integration;
- the timber beam elements (floor joists, roof rafters and ridge beam) and the RC ring beam were modelled with "Class-III Beams 3D" (CLS3B3) curved, three-node, three-dimensional beam elements (CL18B), which are numerically integrated over their cross-section and along their axis.

3.3. Characteristics of numerical models

The mechanical behaviour of the masonry – the only material considered with a nonlinear behaviour – has been modelled using the Total Strain-based Crack (TSC) formulation, originally proposed by Vecchio & Collins [20], which can describe both the tensile and the compressive behaviour with one stress-strain relationship. According to [18] the TSC model is one of the most commonly used for masonry-related simulations.

In order to use the TSC constitutive model in DIANA, the user usually must supply the following parameters: Young's modulus (E); Poisson's ratio (ν); mass density (ρ); tensile strength (f_t); mode-I tensile fracture energy (G_{f_t}); compressive strength (f_c); and compressive fracture energy (G_{f_c}). The fracture energy is divided by the crack bandwidth (h). Regarding the shear modulus (G), it is automatically calculated by the software ($G = E/[2(1 + \nu)]$).

Regarding the damage due to tensile cracking, it is possible to opt for a fixed crack model or a rotating crack model, whose main difference lies in the crack orientation during the inelastic process. Even though it is generally recommended to use the latter for URM structures [18], a fixed crack orientation (with a shear retention factor equal to 0.1) has been considered in this work. The reason lies in the fact that the rotating crack model has led to excessively soft post-peak behaviours during the pushover analyses, diverging excessively from the experimental results.

For the stiffness adaptation of the analysis model, DIANA allows the user to choose a predefined softening function (inelastic constitutive laws) with appropriate parameters [19]. In the present work, it has been chosen the parabolic and the exponential functions, for the compression and tension softening, respectively. This choice has been successfully used in many applications in complex masonry structures [21,22]. In addition, the choice for not considering the experimental characterization of the masonry lies mostly on the fact that experimental test campaigns devoted to the characterisation of masonry subjected to tension are rare. Since the tensile strength of masonry is very low, such experimental tests are difficult to perform.

The remaining materials (timber and RC) were modelled considering a linear elastic isotropic behaviour.

Table 1 summarises the calibrated mechanical properties of the masonry walls and timber diaphragms implemented in the Tremuri macroelement model of Building 3 from Penna et al. [10]. In this table are also included the results from the complementary characterization tests on wallettes performed during the experimental campaign at EUCENTRE [23]. According to Penna et al. [10] the noticeable difference between the experimental and the calibrated value of the Young's modulus may have been caused by the different boundary conditions of the piers during the tests (due to the presence of the RC ring beam) and by the presence of through stones at the lateral ends of the piers, which may have caused the differences between the slender and squat piers.

Table 1. Mechanical properties used in the Tremuri numerical model of Building 3 from Penna et al. [10]

		Experimental characterisation tests of wall specimens [23]	Building 3 [10]	Units
Masonry walls	*Linear material properties:*			
	- Young's modulus, E	2550 (2273 – 2826)	1700	MPa
	- Poisson's ratio, ν	ν_{hor}=0.19, ν_{transv}=0.15	0.2	-
	- Mass density, ρ	2250	2250	kg/m³
	Tensile behaviour (tensile curve: exponential)			
	- Tensile strength, f_t	0.137 (0.112 – 0.161)	0.138	MPa
	- Mode-I tensile fracture energy, G_{f_t}	n. a.	n. a.	
	Compressive behaviour (compression curve: parabolic)			
	- Compressive strength, f_c	3.28 (3.07 – 3.48)	4.5	MPa
	- Compressive fracture energy, G_{f_c}	n. a.	n. a.	
Composite first floor diaphragm	*Linear material properties:*			
	- Young's modulus, E_x, E_y		30 000, 30 000	MPa
	- Poisson's ratio, ν		0.3	-
	- Mass density, ρ		n. a.	
Composite roof diaphragm	*Linear material properties:*			
	- Young's modulus (transversal, longitudinal, and average), E_x, E_y, E_{mean}		21 800, 11 800, 16 800	MPa
	- Poisson's ratio, ν		0.3	-
	- Mass density, ρ		n. a.	

Notes:
- The numbers in brackets refer to the associated range of values obtained experimentally.
- The symbols ν_{hor} and ν_{transv} refer to the Poisson's coefficients in the horizontal and in the transverse directions relatively to the plane of the wall specimens, respectively.
- The symbols E_x and E_y refer to the Young's modulus associated to the transversal and longitudinal directions, respectively. The symbol E_{mean} is the mean value of the Young's modulus associated to the transversal and longitudinal directions.

3.4. Calibration based on modal analysis

The first step of the numerical analysis carried out in the present paper concerns the attainment of the first numerical global modal shapes and corresponding frequencies through a numerical eigenvalue analysis with the DIANA software, and their calibration with the ones identified experimentally through ambient vibration tests, table random weak motion tests and a dynamic test at increasing nominal PGA levels (for further details, see [8,9,13]).
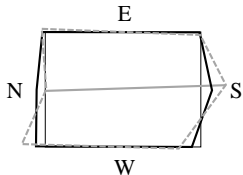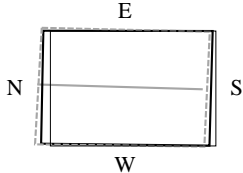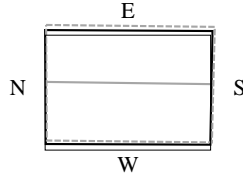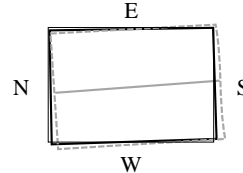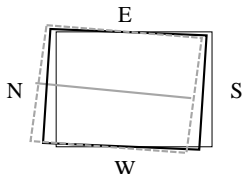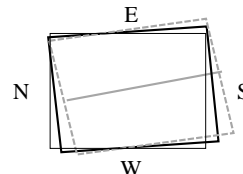
The calibration process was done by changing the value of the Young's modulus assigned to the URM walls (which is the parameter with the highest influence on the dynamic behaviour), by trial-and-error, until a acceptable agreement between the first three natural frequencies measured experimentally and the ones obtained numerically was registered. The obtained frequencies, as well as the relative differences between the experimental and numerical results, are summarised in Fig. 6.

Moreover, the following aspects should be noted regarding the calibration of the numerical models based on the global vibration modes:

(i)   The calibration has been carried out based primarily on the first global mode, which is prevalently longitudinal (parallel to the seismic input applied experimentally);

(ii)   The lack of evidence of the second mode of vibration during the random vibration tests of Building 3 is due to the fact that the base motion was imposed to the structure only in one

direction (uniaxial shaking table) and this has significantly influenced the identification of the modes of vibration [8];

(iii) Two different calibrated values for the masonry Young's modulus have been considered in the present study:

- In the first model updating, a higher value has been used ($E = 923\ MPa$) for the calibration of the vibration modes, to capture better the higher initial elastic-linear stiffness of the models (i.e., the slope of the pushover curve immediately after the instant when the pushover starts). Herein, the calibration of the modes was based on the dynamic properties estimated through dynamic identification tests. These tests correspond to forced vibration tests with very low amplitude, which does not cause damage nor non-linear behaviour. As the experimental models presented minor initial damage, some crack opening (non-linear behaviour) can occur even for the dynamic identification tests, causing a decrease in the calibrated Young´s modulus ($923\ MPa$), with respect to the value obtained from the material characterization tests ($2550\ MPa$, see Table 1). Although in the second validation of the numerical modelling a lower value was adopted ($E = 500\ MPa$), this calibration was fundamental to validate the mode shapes;

- In the second calibration (relevant for the next subsection), a lower value has been used ($E = 500\ MPa$) for the calibration of the global stiffness to capture the overall shape of the experimental pushover curves up to the yield point. Herein, the calibration was based on the seismic tests, which involved the application of accelerograms with increasing amplitude and with higher action than the used in the dynamic identification tests. Thus, due to the existing initial damage, a higher crack opening (non-linear behaviour) was expected in the seismic tests, even for the first tests with the lowest seismic amplitudes. In this way, a lower Young´s modulus ($500\ MPa$) is considered plausible. This is consistent with the recommendations from the Italian structural code (published in the NTC 2008 document and in the relevant guideline Circ. NTC08) [24] which states that, in order to consider the material in cracked conditions, a Young´s modulus equal to half of the of the real one (undamaged material) should be adopted for the seismic assessment of masonry buildings.

		Mode 1	Mode 2	Mode 3
Building 1	Experimental modal identification results (before the dynamic test at 0.05 g) [13]	$f = 7.35\ Hz$	n. a. $f = 8.65\ Hz$	n. a. -
	Numerical eigenvalue analysis (DIANA)			
	$E = 500\ MPa$ $E = 923\ MPa$	$f = 5.33\ Hz\ (\Delta f = -27.48\%)$ $f = 7.09\ Hz\ (\Delta f = -3.45\%)$	$f = 5.52\ Hz\ (\Delta f = -39.31\%)$ $f = 7.13\ Hz\ (\Delta f = -17.57\%)$	$f = 8.25\ Hz$ $f = 10.94\ Hz$
Building 3	Experimental modal identification results (before the dynamic test at 0.05 g) [8]	$f = 7.35\ Hz$	n. a. -	$f = 14.05\ Hz$

E

N | S   N | S   N | S

W   W   W

Numerical eigenvalue analysis (DIANA)

$E = 500\ MPa$ $f = 5.75\ Hz\ (\Delta f = -21.71\%)$ $f = 5.88\ Hz$ $f = 9.21\ Hz\ (\Delta f = -34.46\%)$
$E = 923\ MPa$ $f = 7.41\ Hz\ (\Delta f = 0.82\%)$ $f = 7.64\ Hz$ $f = 12.10\ Hz\ (\Delta f = -13.88\%)$

—— undeformed   ▬▬ floor level   ••••• roof gutter level   ▬▬ ridge beam
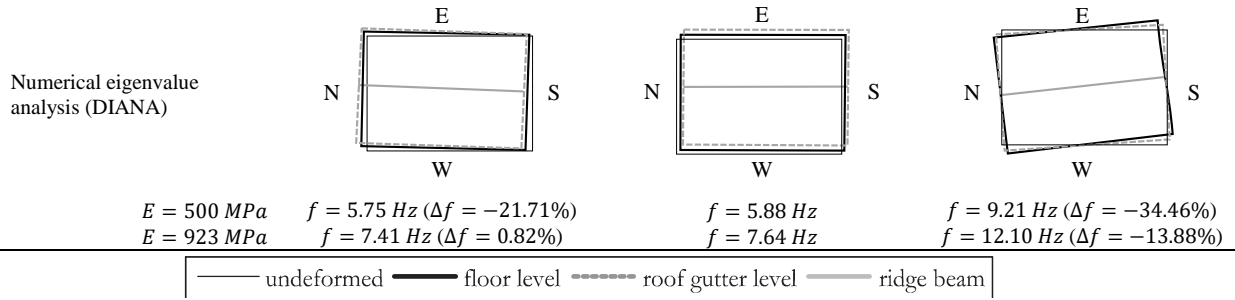
Fig. 6. Mode shapes and frequencies of Building 1 and Building 3

Based on these results, it is possible to conclude that both the modal shapes and frequencies of the numerical models (considering $E = 923\ MPa$) match satisfactorily with those obtained experimentally. Similarly to the experimental observations from [13], the first mode of vibration of Building 3 was dominated by the in-plane first mode response of the longitudinal walls and by the torsion of the floor and roof diaphragms, hence depicting a more "global" type of response of the structure. In contrast, Building 1 revealed a higher tendency of the longitudinal walls to respond independently from each other, given the lack of connection between the walls and diaphragms.

The obtained first mode shapes will serve as the basis for the definition of the horizontal acceleration distribution patterns in the further coming pushover analysis of the case study buildings.

3.5. Calibration based on pushover analysis

The next step of the numerical analysis regards the execution of the pushover analysis, definition of the pushover curves and damage patterns, and the respective comparison with the ones obtained experimentally for Buildings 1 and 3, in both the positive and negative directions of the Y-axis.

As proposed in the current building codes, such as EC8 [25], the nonlinear static analysis was performed subjecting the structures to a modal force pattern to represent the dynamic amplification attained in the experimental tests, given the distribution of accelerations proportional to the first mode of vibration.

The calibrated mechanical properties of the structural materials used in the DIANA numerical models of Buildings 1 and 3 are summarised in Table 2.

Table 2. Mechanical properties used in the DIANA numerical models

		Building 1	Building 3	Units
Masonry walls	*Linear material properties:*			
	- Young's modulus, E	500	500	MPa
	- Poisson's ratio, ν	0.2	0.2	-
	- Mass density, ρ	2250	2250	kg/m³
	Tensile behaviour (tensile curve: exponential)			
	- Tensile strength, f_t	0.180	0.180	MPa
	- Mode-I tensile fracture energy, G_{f_t}	50	50	N/m
	Compressive behaviour (compression curve: parabolic)			
	- Compressive strength, f_c	1	1	MPa
	- Compressive fracture energy, G_{f_c}	6000	6000	N/m
Timber used in the floor and roof diaphragms (non-structural planar elements)	*Linear material properties:*			
	- Young's modulus, E	500	16 800	MPa
	- Poisson's ratio, ν	0.3	0.3	-
	- Mass density, ρ	600	600	kg/m³
Timber used in the floor joists, roof rafters, ridge beam and lintels (structural beam elements)	*Linear material properties:*			
	- Young's modulus, E	10 000	10 000	MPa
	- Poisson's ratio, ν	0.3	0.3	-
	- Mass density, ρ	600	600	kg/m³
RC used in the ring beam and collaborating slab (C25/30)	*Linear material properties:*			
	- Young's modulus, E		28 000	MPa
	- Poisson's ratio, ν		0.2	-
	- Mass density, ρ		2400	kg/m³
Weight of the floor level 1		340.08	372.03	kN
Weight of the floor level 2		308.81	351.44	kN
Total weight of the building		648.89	723.47	kN

The pushover curves were calibrated based on modifications of the mechanical properties of the masonry walls.

The differences between the calibrated/experimental values from Table 2 and the ones from Table 1 may be justified by the inherent differences between the experimental models (full-scale prototype buildings) and the FEM, such as the influence of the boundary conditions, the presence of damage in the prototype buildings, and/or the considered masonry constitutive models which required additional parameters not defined beforehand (namely the tensile and compressive fracture energy).

Once the global stiffness was calibrated (considering $E = 500 \, MPa$), the calibration of the maximum capacity and the post-peak response has been carried out. In general terms, the Young's modulus governs the global stiffness; the tensile strength, the mode-I tensile fracture energy and the compressive strength govern the maximum capacity; and, the compressive fracture energy governs the post-peak softening behaviour.

Regarding the properties of the timber elements, three different values for the Young's modulus have been used. The structural beam elements (floor joists, roof rafters, ridge beam and lintels) have been modelled considering $E = 10000 \, MPa$, which is the typical Young's modulus for pinewood (along grain). The non-structural planar elements (timber planks) have been modelled considering two different values for the Young's modulus, one for each building. The reduced value considered in the timber diaphragms of Building 1 ($E = 500 \, MPa$) has been deliberately manipulated to capture the differences in terms of capacity between Buildings 1 and 3. This difference is justified by the fact that the timber planks are not effectively connected to each other, whereby a monolithic behaviour might not be realistic to de assured in practice. In contrast, the higher value considered for Building 3 ($E = 16800 \, MPa$) corresponds to the mean value of the Young's modulus associated to the transversal and longitudinal directions used by Penna et al. [10], and reflects the strengthening action of the addition of the RC reinforcement layer over the existing timber slab.

The obtained numerical results (pushover curves) – correspondent to the average of the four corners at the roof level – are depicted in Fig. 7, for both building prototypes and for both pushover orientations. These results are compared with the ones obtained from the EUCENTRE experimental campaign performed by Magenes et al. (2010b), and with the numerical results of Building 3 from Penna et al. (2016) using the Tremuri software (both correspondent to the average displacement at roof level [8,10,13]).
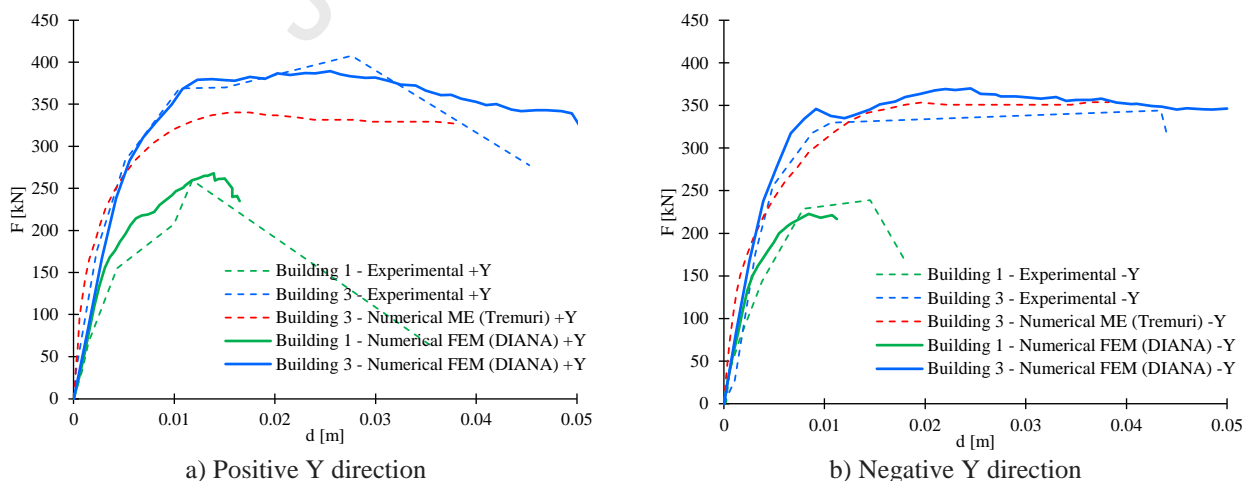

a) Positive Y direction b) Negative Y direction

Fig. 7. Pushover curves for Buildings 1 and 3 in the positive and negative directions of the Y-axis

In addition, Table 3 includes the relative differences between the numerical results from Diana (FEM) and from Tremuri (EFM) (from Magenes et al. (2010b)) and the experimental results from EUCENTRE test campaign, in terms of capacity (F_y), stiffness (F_y/d_y), and ductility ratio (d_u/d_y)

for both orientations of force application (+Y and -Y). The values present in this table have been obtained following the methodology explained in Section 4.2.

Table 3. Comparison of the numerical results from Diana and Tremuri with the experimental results from EUCENTRE

			Capacity (Fy)	Stiffness (Fy/dy)	Ductility ratio (du/dy)
(+Y)	Building 1	(Diana)/(Experimental)-1	4.9%	29.3%	1.3%
	Building 3	(Diana)/(Experimental)-1	2.7%	-12.4%	-12.0%
		(Tremuri)/(Experimental)-1	-11.2%	13.9%	21.5%
(-Y)	Building 1	(Diana)/(Experimental)-1	-4.8%	33.0%	-9.9%
	Building 3	(Diana)/(Experimental)-1	1.4%	29.5%	-4.9%
		(Tremuri)/(Experimental)-1	2.1%	6.2%	-5.6%

The pushover curves obtained with the software DIANA using a FEM approach show a good agreement with the ones obtained experimentally, corroborating the fact that the inclusion of the RC strengthening elements has notably increased the seismic response of the building in terms of capacity and stiffness. Moreover, the results presented in Table 3 show that the relative differences between the numerical and experimental results obtained for Building 3 are generally inferior for the case of the FEM using the software DIANA (except in terms of stiffness in the -Y orientation), therefore validating the performed numerical analysis.

Finally, thanks to the ability of the FEM to capture damage patterns, one important step was the comparison of the damage patterns detected experimentally for the Building 3 (the only building to which a detailed survey of the crack patterns has been done) with the ones obtained numerically.

It should be noted that the prototype of Building 3 has suffered slight damage during the transportation to the shaking table, due to the deformation of the foundation pad [8].

The comparison of the results is illustrated in Fig. 8. Herein, the damage patterns obtained in DIANA are expressed by means of the elements' crack widths computed for the local direction 1 (Ecw1) and considering the maximum value across the 5 layers of each element.
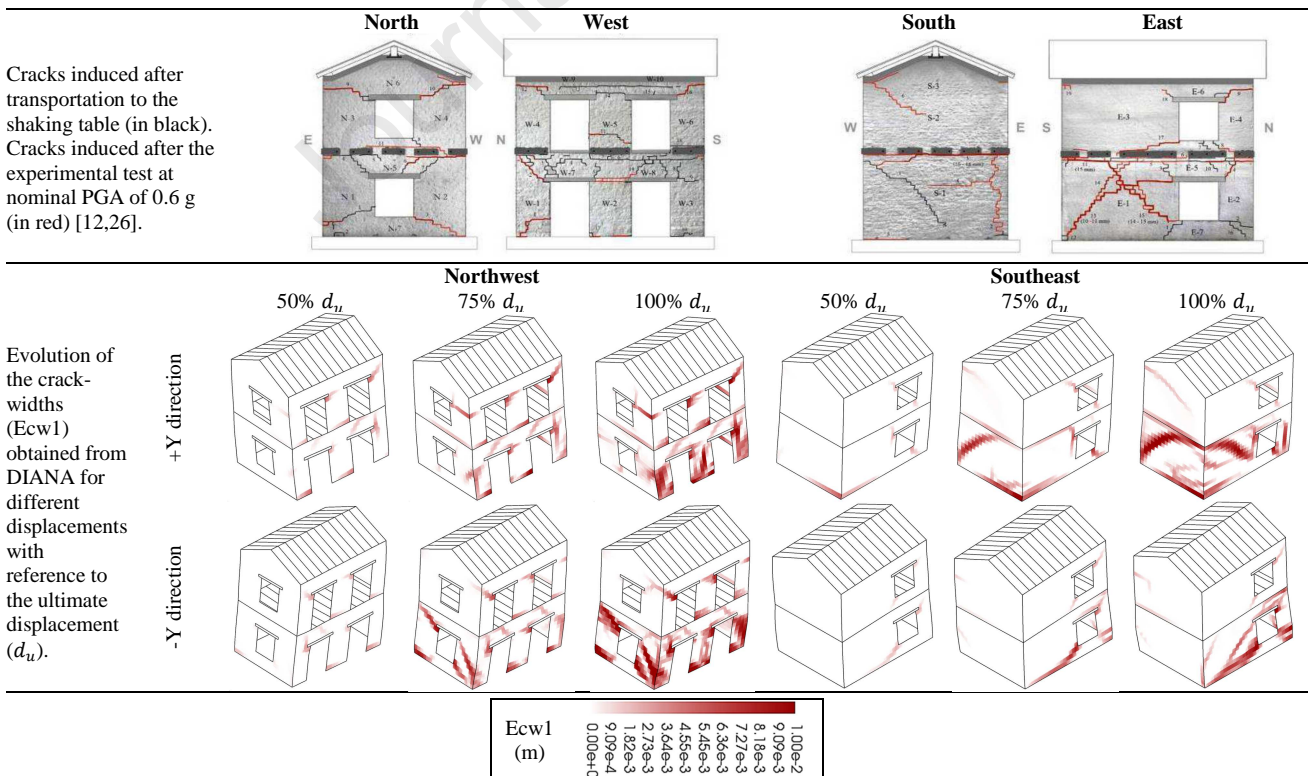

Fig. 8. Damage patterns of Building 3 from the experimental and numerical analysis

Despite the undesirable influence of the existing damages prior to the experimental tests, which might have influenced the final experimental results, it is observable a satisfactory agreement between the numerical and experimental damage patterns. It is visible significant shear cracks at the floor level 1 on the stiffer and stronger longitudinal wall (with two openings) oriented along the shaking direction. In the other longitudinal wall, with more openings, the damage was mainly associated with rocking response of top storey piers. Regarding the transversal walls, similar damage is also present due to the torsional action evidenced by the fundamental vibration modes, motivated by the geometric asymmetries of the building.

4. Analysis of strengthening interventions with RC

4.1. Pushover analyses of strengthened buildings

Once calibrated the numerical models corresponding to the EUCENTRE Buildings 1 and 3, four additional building models have been considered in order to analyse the influence of the strengthening interventions applied in Building 3, separately. Therefore, the numerical cases that will be analysed in the present section are the following (and schematically illustrated in Fig. 9):

- OB – Original Building (corresponding to EUCENTRE Building 1);
- SB1 – Strengthened Building 1, which consists of the OB strengthened with an RC ring beam inserted at the roof level;
- SB2 – Strengthened Building 2, which consists of the OB strengthened with an RC collaborative reinforcement layer on the first-floor diaphragm;
- SB3 – Strengthened Building 3, which consists of the OB strengthened with a reinforcement layer on the roof diaphragm (multi-layer plywood panels);
- SB4 – Strengthened Building 4, which consists in the OB strengthened with an RC collaborative reinforcement layer on the first-floor diaphragms and reinforcement on the roof diaphragm (multi-layer plywood panels);
- SB5 – Strengthened Building 5, which consists of the OB strengthened with the combination of all previous strengthening elements (corresponding to EUCENTRE Building 3).
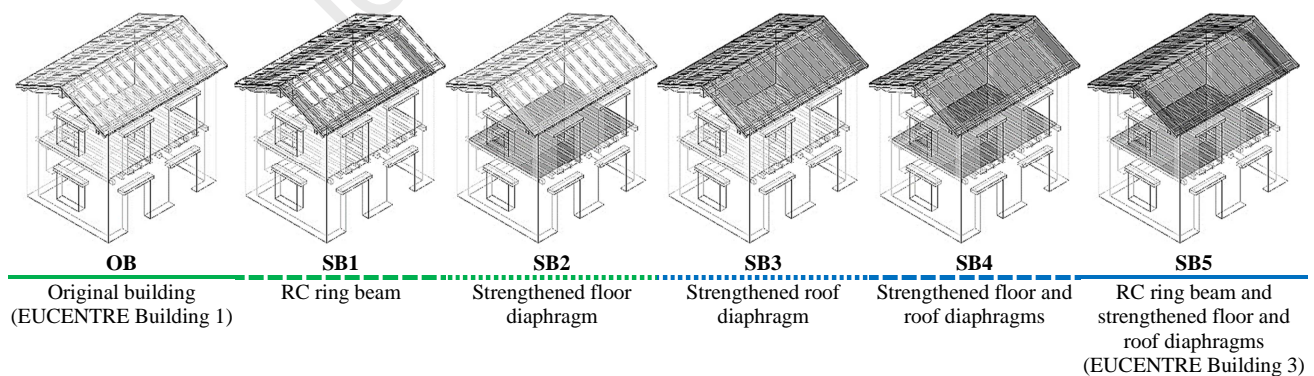

OB	SB1	SB2	SB3	SB4	SB5
Original building (EUCENTRE Building 1)	RC ring beam	Strengthened floor diaphragm	Strengthened roof diaphragm	Strengthened floor and roof diaphragms	RC ring beam and strengthened floor and roof diaphragms (EUCENTRE Building 3)

Fig. 9. Scheme of the considered cases (RC elements shaded in grey)

Similarly to the previous section, the obtained numerical results (pushover curves) – correspondent to the average of the four corner angles at the roof level – are depicted in Fig. 10, for the six considered cases and for both pushover Y directions.
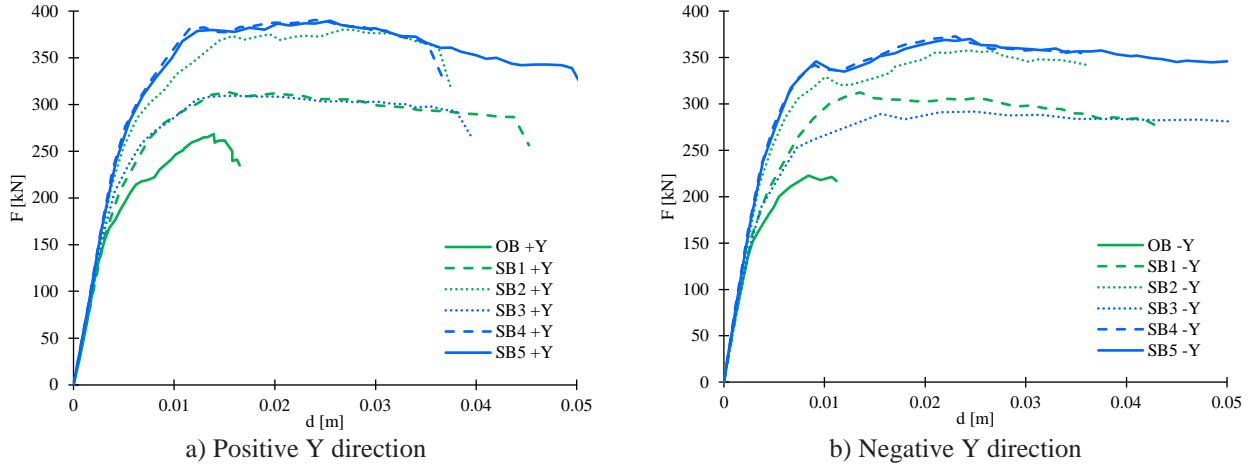
Fig. 10. Pushover curves for the OB and SB considered cases

The obtained pushover curves suggest that, for the considered cases, all strengthening interventions have improved the global seismic response of the original building (OB). The best result, as expected, corresponds to the SB5 where all strengthening elements are included. However, very similar results have been obtained for the SB4, and to a slightly lesser extent, for the SB2, although these showed a shorter post-peak branch (i.e., less ductility). This fact suggests that the presence of the ring beam in the SB5 is responsible for the additional ductility when compared with SB4 and SB2. Another pair of cases that showed very similar results (particularly in the positive Y direction) correspond to the SB1 and SB3, which in terms of global seismic response are located half-way between the OB and the SB5.

4.2. Seismic performance assessment

Once obtained the pushover curves for all cases, the target displacements have been determined from the elastic response spectrum in accordance with the Informative Annex B of EC8 [25]. For such purpose, the seismic action has been defined with the following parameters:

- Type 1 spectrum;
- Ground acceleration $a_{gR} = 2.94\ m/s^2 = 0.3$ g. This value corresponds to the maximum peak ground acceleration according to the Italian seismic hazard map (Italian Seismic National Annex Ordinanza PCM del 28 Aprile 2006 n.3519, All.1b);
- Importance factor $\gamma_1 = 1$;
- Soil type A;
- Damping correction factor $\eta = 1$ (for 5% viscous damping).

The idealised elastic-perfectly plastic force-displacement relationships (bilinear pushover curves) of the numerical cases analysed are illustrated in Fig. 11, and have been obtained by converting the pushover curve from the original Multi Degree of Freedom (MDoF) system into an equivalent Single Degree of Freedom (SDoF) system, according to the method described by Correia Lopes et al. [27] (based on the N2 Method, originally proposed by Fajfar (1999)), which corresponds to the iterative procedure recommended in the Annex B of Eurocode 8 – Part 1 [25].

The vertices of these curves represent the yield displacement limit point (d_y, F_y) and the target displacement point (d_t, F_y).

Regarding the ultimate displacement (d_u), it has been taken as the roof displacement at which total lateral resistance (base shear) has dropped below 90% of the peak resistance of the structure. This percentage differs from the one recommended in Annex C of Eurocode 8 – Part 3 [29] because, in the present analysis, all obtained pushover curves of the strengthened building models showed a significant post-peak branch with a moderate and gradual softening behaviour, which was insufficient to attain a drop of 80% of the peak resistance as suggested in EC8.
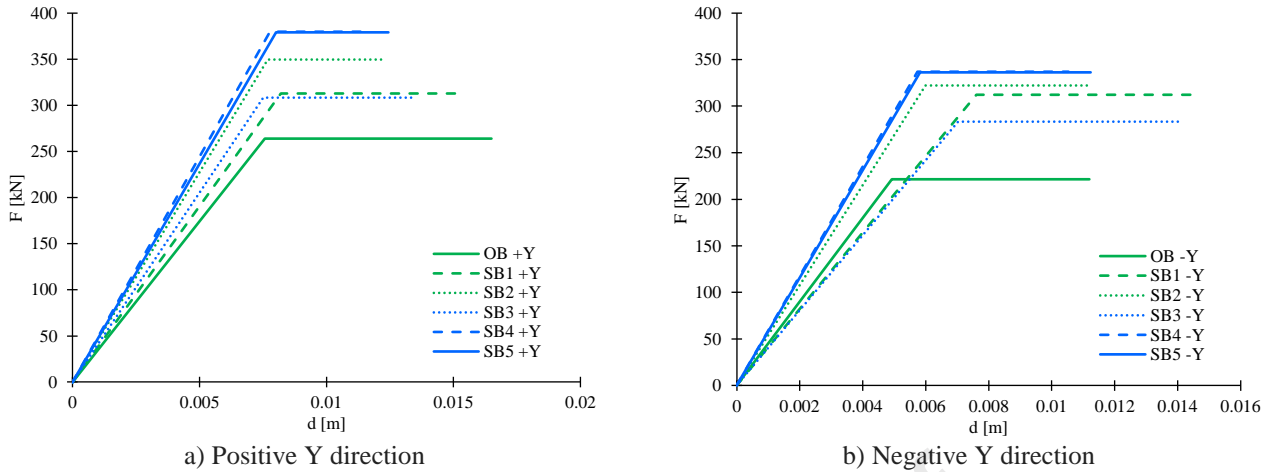
a) Positive Y direction   b) Negative Y direction
Fig. 11. Idealised elastic-perfectly plastic force-displacement relationships

Table 4 includes the relative differences between the models of the buildings with the strengthening elements (SB1, SB2, SB3, SB4 and SB5) and the original building (OB), in terms of capacity (F_y), stiffness (F_y/d_y), and ductility ratio (d_u/d_y) for both orientations of force application (+Y and -Y). This table also includes the same comparisons between the experimental results from the EUCENTRE experimental campaign.

Table 4. Comparison of the results obtained from the models with and without the strengthening elements

			Capacity (Fy)	Stiffness (Fy/dy)	Ductility ratio (du/dy)
(+Y)	Numerical (DIANA)	(SB1)/(OB)-1	18.5%	9.3%	123.8%
		(SB2)/(OB)-1	32.5%	30.5%	118.8%
		(SB3)/(OB)-1	16.8%	17.9%	132.6%
		(SB4)/(OB)-1	43.9%	40.1%	107.3%
	Numerical (DIANA)	(SB5)/(OB)-1	43.6%	35.9%	144.4%
	Experimental	(SB5)/(OB)-1	46.8%	100.5%	203.9%
(-Y)	Numerical (DIANA)	(SB1)/(OB)-1	40.9%	-8.8%	98.3%
		(SB2)/(OB)-1	45.4%	19.5%	241.7%
		(SB3)/(OB)-1	27.9%	-10.4%	313.4%
		(SB4)/(OB)-1	52.1%	30.4%	245.9%
	Numerical (DIANA)	(SB5)/(OB)-1	51.8%	28.5%	321.1%
	Experimental	(SB5)/(OB)-1	42.5%	31.9%	160.1%

It should be noticed that these comparisons are intrinsically dependent on the method used to obtain the bilinear idealisation of the pushover curves, from which the quantities F_y, d_y, and d_t are extracted.

According to the obtained results, the addition of the RC structural elements has increased the capacity, the stiffness (except for the two cases in red in Table 4) and the ductility of the structure. It can also be observed that the numerical results from DIANA seem consistent with those from the EUCENTRE experimental campaign (see the cases of SB5), particularly in terms of capacity, where the relative differences between the model SB5 and the original building (OB) are very similar.

In addition, Fig. 12 contains the representation of the scale factor (γ) for the reference ground acceleration as a function of the control node displacement (d). This method allows to visualise the target displacement (horizontal axis) for other values of the seismic action apart from the reference ground acceleration (a_{gR}). (For further details about the method see [27].)

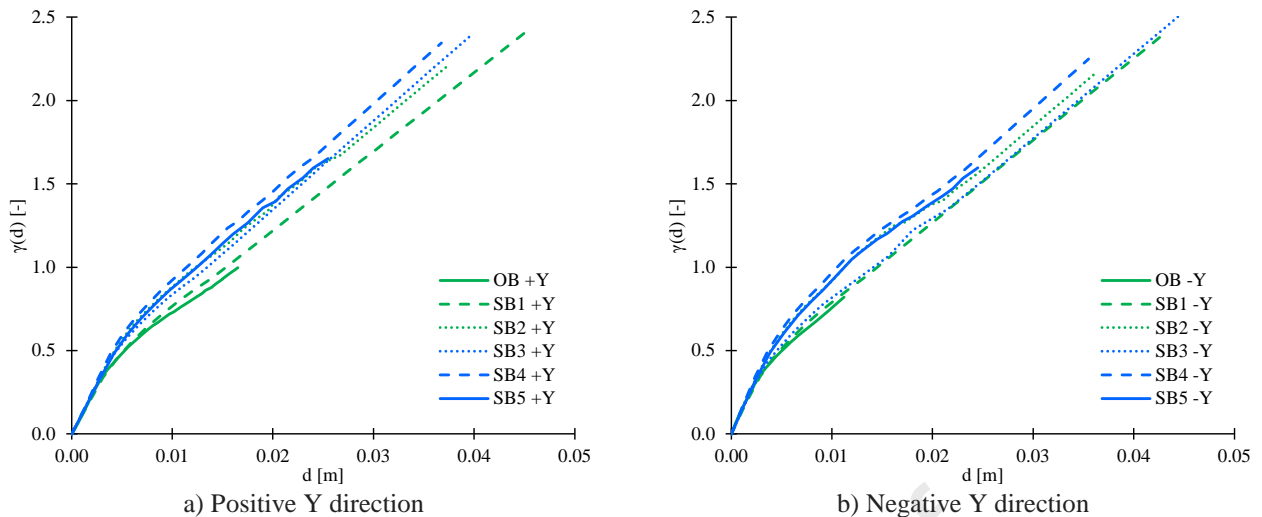a) Positive Y direction | b) Negative Y direction

Fig. 12. Relationship between the target displacement of the SDoF system and the scale factor for the seismic action

According to the obtained results, the introduction of the RC elements has resulted in a significant reduction of the target displacements, regardless of the considered seismic demand, since the curves of the strengthened buildings are steeper than the one of the original building.

5. Conclusions

The present work has examined the influence of different strengthening interventions with RC in existing URM buildings based on pushover analyses comparison.

The pushover curves obtained with the software DIANA have been calibrated based on the experimental results from the shaking table tests performed at EUCENTRE on full-scale stone masonry buildings. The variability of the mechanical properties may have influenced the accuracy of the numerical results. In addition, since the level of monolithicity and uniformity of the walls plays an important role on the seismic response of the masonry buildings, any unrepaired crack on the walls or heterogeneity in the stone fabric and laying could have affected the experimental test results and, consequently, the calibration of the numerical models.

The obtained results, for the considered case study building, have corroborated the experimental results, showing that the inclusion of the RC strengthening elements has increased the seismic response of the building in terms of capacity, stiffness, and ductility, compensating the unfavourable effect of the additional mass. Moreover, it has been observed that the addition of reinforcement layers on both diaphragms (or on the first-floor diaphragm only) gives similar results to the case with all the considered strengthening actions. Consequently, the insertion of an RC ring beam and the addition of a reinforcement layer over the roof diaphragm have proven to be less efficient techniques. These results reveal that the use of RC, specifically in the execution of a perimetral ring beam or as a layer in a collaborative floor slab, provided that they are not executed in an extensive and indiscriminate manner, can be seen as a retrofitting option for common residential building stock, aiming at the mitigation of the seismic vulnerability and at the persuasion against more ruthless decisions, such as demolition. Nonetheless, each case must be assessed individually to evaluate that such intervention strategies, and namely the use of RC, are compatible and executable (e.g.: the assessment of roof truss systems, the capacity of the existing timber floor diaphragm, floor to wall connections, etc.)

Finally, a larger amount of experimental and numerical data should also be analysed in the future with specific reference to different diaphragm stiffnesses, wall-to-floor connections, material properties, and building geometries, for the comparison of the effectiveness of the different strengthening strategies applied on the considered case-study building.

6. Acknowledgements

7. References

[1]   G. Correia Lopes, R. Vicente, T.M. Ferreira, M. Azenha, Intervened URM buildings with RC elements: typological characterisation and associated challenges, Bull. Earthq. Eng. 17 (2019) 4987–5019. doi:10.1007/s10518-019-00651-y.

[2]   M. Tomaževič, C. Modena, T. Velechovsky, P. Weiss, The effect of reinforcement on the seismic behavior of masonry buildings with mixed structural systems: an experimental study, in: Proc. 9th Eur. Conf. Earthq. Eng., Moscow, Russia, 1990.

[3]   D. Jurukovski, L. Krstevska, R. Alessi, P.P. Diotallevi, M. Merli, F. Zani, Shaking table tests of three four-storey brick masonry models: Original and strengthened by RC core and by RC jackets, in: 10th World Conf. Earthq. Eng., Balkema, Rotterdam, 1992: pp. 2795–2800.

[4]   M. Dolce, F.C. Ponzo, A. Goretti, C. Moroni, F. Giordano, G. De Canio, R. Marnetto, 3D Dynamic Tests on 2/3 Scale Masonry Buildings Retrofitted With Different Systems, Proc. 14th World Conf. Earthq. Eng. (2008).

[5]   N. Mazzon, M.R. Valluzzi, T. Aoki, E. Garbin, G. De Canio, N. Ranieri, C. Modena, Shaking Table Tests on Two Multi-leaf Stone Masonry Buildings, 11th Can. Mason. Symp. (2009).

[6]   J.K. Bothara, R.P. Dhakal, J.B. Mander, Seismic performance of an unreinforced masonry building: An experimental investigation, Earthq. Engng Struct. Dyn. (2010) 45–68. doi:10.1002/eqe.932.

[7]   E. Vintzileou, C. Mouzakis, C.E. Adami, L. Karapitta, Seismic behavior of three-leaf stone masonry buildings before and after interventions: Shaking table tests on a two-storey masonry model, Bull. Earthq. Eng. 13 (2015) 3107–3133. doi:10.1007/s10518-015-9746-x.

[8]   I. Senaldi, G. Magenes, A. Penna, A. Galasco, M. Rota, The effect of stiffened floor and roof diaphragms on the experimental seismic response of a full-scale unreinforced stone masonry building, J. Earthq. Eng. 18 (2014) 407–443. doi:10.1080/13632469.2013.876946.

[9]   G. Magenes, A. Penna, A. Galasco, A Full-Scale Shaking Table Test on a Two-Storey Stone Masonry Building, 14th Eur. Conf. Earthq. Eng. (2010) 384.

[10]   A. Penna, I.E. Senaldi, A. Galasco, G. Magenes, Numerical Simulation of Shaking Table Tests on Full-Scale Stone Masonry Buildings, Int. J. Archit. Herit. 10 (2016) 146–163. doi:10.1080/15583058.2015.1113338.

[11]   A. Penna, G. Magenes, I. Senaldi, A. Galasco, Equivalent-Frame Macro-Element Simulation of Shaking Table Tests on Unreinforced Stone Masonry Buildings With Strengthening Interventions, in: F. Peña, M. Chávez (Eds.), SAHC2014 – 9th Int. Conf. Struct. Anal. Hist. Constr., 2014.

[12]   G. Magenes, A. Penna, M. Rota, A. Galasco, I. Senaldi, Shaking table test of a full scale stone masonry building with stiffened floor and roof diaphragms, in: 15th World Conf. Earthq. Eng., Lisbon, Portugal, 2012: pp. 24–28.

[13]   G. Magenes, A. Penna, I.E. Senaldi, M. Rota, A. Galasco, Shaking table test of a strengthened full-scale stone masonry building with flexible diaphragms, Int. J. Archit. Herit. 8 (2014) 349–375. doi:10.1080/15583058.2013.826299.

[14]   S. Lagomarsino, A. Penna, A. Galasco, TREMURI program: seismic analysis program for 3D masonry buildings. Theory and user manual., (2006).

[15]   Autodesk, Revit, (2019).

[16]   DIANA FEA BV, DIANA FEA, (2019).

[17] DIANA FEA BV, Using the Revit plugin v17.0 with DIANA Finite Element Analysis, (n.d.).

[18] P.B. Lourenço, J.M. Pereira, Seismic Retrofitting Project: Recommendations for Advanced Modeling of Historic Earthen Sites, J. Paul Getty Trust and TecMinho, 2018.

[19] DIANA FEA BV, DIANA Finite Element Analysis Theory Manual, (2017). https://dianafea.com/manuals (accessed November 8, 2020).

[20] F.J. Vecchio, M.P. Collins, The modified compression field theory for reinforced concrete elements subjected to shear, J. Am. Concr. Inst. 83 (1986) 219–231. doi:10.14359/10416.

[21] P.B. Lourenço, Recent Advances in Masonry Modelling: Micromodelling and Homogenisation, in: Multiscale Model. Solid Mech., Imperial College Press, London, 2009.

[22] M. Salvalaggio, P. Roca, M.R. Valluzzi, F. Lorenzoni, Finite element micro-modeling for the characterization of inclined head joints archaeological masonry: The case of Villa Diomede in Pompeii, COMPDYN 2017 - Proc. 6th Int. Conf. Comput. Methods Struct. Dyn. Earthq. Eng. 1 (2017) 2460–2469. doi:10.7712/120117.5581.17486.

[23] G. Magenes, A. Penna, A. Galasco, M. Rota, Experimental characterisation of stone masonry mechanical properties, in: 8th Int. Mason. Conf. 2010, 2010.

[24] IBCC, Italian Building Code Commentary: Circolare n. 617 del 02.02.2009: Istruzioni per l'applicazione delle "Norme tecniche per le costruzioni" di cui al D.M. 14 gennaio 2008, GU n. 47 del 26-2-2009 - Suppl. Ordinario n.27, Ministero delle Infrastrutture e dei Trasporti, Roma [in Italian], 2009. doi:10.1016/j.ssmph.2017.08.008.

[25] CEN, Eurocode 8: Design of structures for earthquake resistance - Part 1: General rules, seismic actions and rules for buildings, Comite Europeen de Normalisation, Brussels, Belgium, 2004. doi:[Authority: The European Union per Regulation 305/2011, Directive 98/34/EC, Directive 2004/18/EC].

[26] G. Magenes, A. Penna, Seismic Design and Assessment of Masonry Buildings in Europe: Recent Research and Code Development Issues, in: 9th Australas. Mason. Conf., Queenstown, New Zealand, 2011: pp. 583–603.

[27] G. Correia Lopes, R. Vicente, T.M. Ferreira, M. Azenha, J. Estêvão, Displacement-based seismic performance evaluation and vulnerability assessment of buildings: The N2 method revisited, Structures. 24 (2020) 41–49. doi:10.1016/J.ISTRUC.2019.12.028.

[28] P. Fajfar, Capacity spectrum method based on inelastic demand spectra, Earthq. Eng. Struct. Dyn. 28 (1999) 979–993. doi:10.1002/(SICI)1096-9845(199909)28:9<979::AID-EQE850>3.0.CO;2-1.

[29] CEN, Eurocode 8: Design of structures for earthquake resistance - Part 3: Assessment and retrofitting of buildings, Comite Europeen de Normalisation, Brussels, Belgium, 2005.

Manuscript title: "*Numerical simulations of derived URM-RC buildings: assessment of strengthening interventions with RC*"

Highlights:

- Mixed URM–RC buildings may be particularly vulnerable to seismic action;
- The complex structural behaviour of mixed URM–RC buildings is understudied;
- Analysis of strengthening interventions with RC in existing URM buildings;
- RC elements can be seen as a retrofitting option to mitigate seismic vulnerability.

Declaration of interests

☒ The authors declare that they have no known competing financial interests or personal relationships that could have appeared to influence the work reported in this paper.

☐The authors declare the following financial interests/personal relationships which may be considered as potential competing interests: